Materials Science in Semiconductor Processing 90 (2019) 1–6

Contents lists available at ScienceDirect

Materials Science in Semiconductor Processing

journal homepage: www.elsevier.com/locate/mssp

Simulation of optimum band structure of HTM-free perovskite solar cells based on ZnO electron transporting layer

Lingyan Lin[a,b], Linqin Jiang[a,b,*], Ping Li[a,b], Baodian Fan[a,b], Yu Qiu[a,b], Fengpo Yan[a,b]

[a] Institute of Advanced Photovoltaics, Fujian Jiangxia University, Fuzhou 350108, China
[b] College of Electronic Information Science, Fujian Jiangxia University, Fuzhou 350108, China

ARTICLE INFO

Keywords:
Graded band gap
SCAPS-1D
Perovskite solar cell
HTM-free

ABSTRACT

Expensive gold electrode and hole transporting material (HTM) currently used in perovskite solar cells are the major economic constraints to the scaling-up of this promising technology. Designing high-efficiency perovskite solar cell with graded band-gap structure to replace HTM and with low-cost electrode is urgently needed for real cell production. In our work numerical simulation of perovskite solar cell with the configuration of FTO/ZnO/$CH_3NH_3Pb(I_{1-x}Br_x)_3$/Carbon is performed using SCAPS-1D program. The band gap of $CH_3NH_3Pb(I_{1-x}Br_x)_3$ absorber is tuned in the range of 1.5 eV to 2.3 eV by variation of the Br doping content. Both the uniform band gap and graded band gap absorber were examined. Based upon the simulated results, a promising efficiency of 17.89% can be realized with a back grading profile that consists of a graded thickness of 50 nm as well as 1.9 eV band gap at back surface. This work will provide guidelines for further efficiency enhancement of low cost perovskite solar cells.

1. Introduction

In the past several years, organic-inorganic metal halide perovskite solar cells have drawn tremendous interest as promising devices for solar energy utilization due to its simple fabrication process and high power conversion efficiency [1–5]. HTM-free perovskite solar cells (PSCs) are also an important type of PSCs because of their simple structure, low cost and improved stability of the device. The perovskite layers can act both as absorbers for light absorption and as hole transport layers for the holes transporting to the back contact. The highest efficiency of HTM-free PSCs reported so far is 8.73% with the structure FTO/ZnO/$CH_3NH_3PbI_3$/Carbon [6], which is substantially lower than the conversion efficiencies of PSCs with HTM. One reason may be that in HTM-free PSCs the lower band gap of $CH_3NH_3PbI_3$ is insufficient to form an enough energy barrier to hinder the transport of minority carriers from absorber to back contact, thereby increasing back surface recombination probability. Recently, the mixed halide perovskite ($CH_3NH_3Pb(I_{1-x}Br_x)_3$) has drawn great attention as light absorber in PSCs because its band-gap energy (E_g) can be tuned in the range of 1.5–2.3 eV by tuning the Br content (x) [7], thus enabling a graded band-gap of the light absorption layer. The band-gap gradient concept is originally coming from CIGS solar cell research. In the CIGS solar cell, high efficiency is achieved by controlling the depth profile of the band gap, which is an approach to further enhance solar spectrum utilization [8,9]. Therefore, in this study, the band gap profiles are optimized by Br doping to enhance the carrier diffusion and photon absorption.

To further enhance the efficiency, the in-depth comprehension of device operation mechanism is of great significance. Numerical simulation is an effective method to predict the influence of physical change on device performance and the feasibility of new design concepts can be tested without actual fabrication. Therefore, in our study, numerical analysis of HTM-free perovskite solar cell are performed to investigate the influence of different band gap profile for the $CH_3NH_3Pb(I_{1-x}Br_x)_3$ absorber layers on the device performance. Firstly, we alter the Br composition uniformly throughout the $CH_3NH_3Pb(I_{1-x}Br_x)_3$ absorber layer to investigate the impact of varied E_g on device performance. Then a graded $CH_3NH_3Pb(I_{1-x}Br_x)_3$ absorber is analyzed, including back grading and double grading. From the simulated result, an optimum absorber band-gap profile of the HTM-free PSCs is proposed, which has not been discussed in literature.

2. Methodology

In this research, device simulation is carried out using SCAPS that developed by University of Gent [10]. The SCAPS program can calculate performance parameters of solar cells by the numerical solutions of the basic semiconductor equations: electron (1) and hole (2) continuity

* Corresponding author at: College of Electronic Information Science, Fujian Jiangxia University, Fuzhou 350108, China.
E-mail address: linqinjiang@fjjxu.edu.cn (L. Jiang).

https://doi.org/10.1016/j.mssp.2018.10.003
Received 31 March 2018; Received in revised form 11 September 2018; Accepted 1 October 2018
Available online 09 October 2018
1369-8001/ © 2018 Elsevier Ltd. All rights reserved.

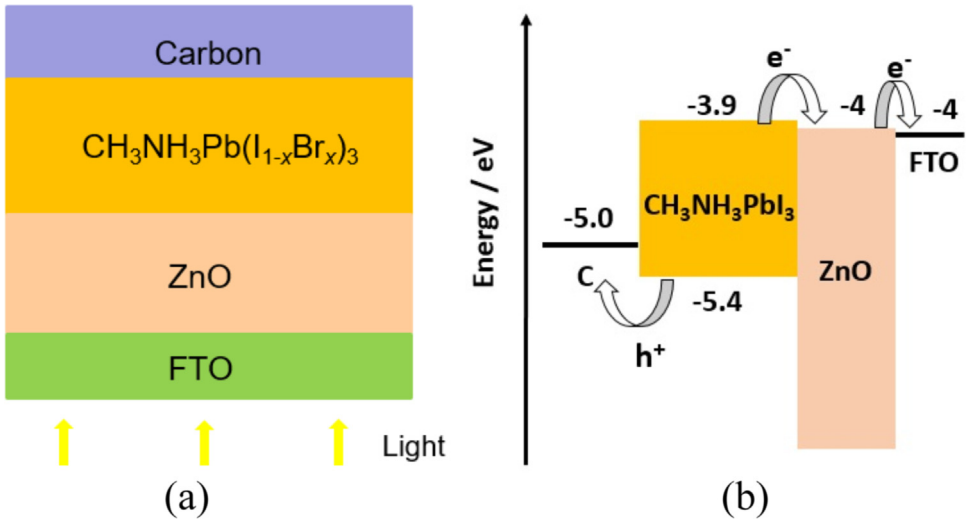

Fig. 1. Schematic diagram (a) and energy band structure (b) of HTM-free PSCs used in the simulation.

equations as well as Poisson Eq. (3), listed as following:

$$\frac{dn_p}{dt} = G_n - \frac{n_p - n_{p0}}{\tau_n} + n_p\mu_n\frac{d\xi}{dx} + \mu_n\xi\frac{dn_p}{dx} + D_n\frac{d^2n_p}{dx^2} \quad (1)$$

$$\frac{dp_n}{dt} = G_p - \frac{p_n - p_{n0}}{\tau_p} - p_n\mu_p\frac{d\xi}{dx} - \mu_p\xi\frac{dp_n}{dx} + D_p\frac{d^2p_n}{dx^2} \quad (2)$$

$$\frac{d}{dx}\left(-\varepsilon(x)\frac{d\psi}{dx}\right) = q\left[p(x) - n(x) + N_d^+(x) - N_a^-(x) + p_t(x) - n_t(x)\right] \quad (3)$$

Through solving the above equation (1) (2) (3), output parameters such as spectral response, energy bands, current voltage characteristics and recombination profile can be calculated. In addition, the grading laws in SCAPS-1D such as exponential, parabolic, logarithmic and linear, can be used to set the composition grading y(x) over a layer, as well as the composition dependence of a property.

The device structure used in our modelling is depicted in Fig. 1, where $CH_3NH_3Pb(I_{1-x}Br_x)_3$ is employed as the absorber and ZnO as the electron transport layer.

ZnO is an ideal material to substitute TiO_2 as electron transport layer because it has the benefit of larger electron mobility, similar bandgap and lower processing temperature compared to TiO_2 [11–13]. Moreover, fluorine doped tin oxide (FTO) and carbon are employed as front contact and back contact, respectively. Table 1 summarizes the physical parameters employed in the simulation, which are adopted from literatures and reported experimental results and their reference are cited. The electron affinity (χ) and energy band gap (E_g) of the $CH_3NH_3Pb(I_{1-x}Br_x)_3$ absorber are varied with Br content (x). E_g of $CH_3NH_3Pb(I_{1-x}Br_x)_3$ is determined by a giant spin–orbit coupling in the conduction band, as indicated by the density functional theory calculations [7]. It was reported that the E_g of $CH_3NH_3PbBr_3$ ($x = 1$) and $CH_3NH_3PbI_3$ ($x = 0$) were 2.3 and 1.5 eV, respectively [7,19,20]. Derived from the position of the Pb-5d orbitals, the χ of $CH_3NH_3PbBr_3$ and $CH_3NH_3PbI_3$ were 3.1 and 3.9 eV, respectively. And an absolute valence band energy of 5.4 eV for $CH_3NH_3PbX_3$ is quoted from Ref. [7]. In our simulation, a linear variation is assumed for the band gap of $CH_3NH_3Pb(I_{1-x}Br_x)_3$ absorber. The dependence of the χ and E_g on Br content (x) was implemented according to equation 3.9–0.8x (eV) and 1.5 + 0.8x (eV), which is assumed that variation in the band gap versus Br content is linear [21]. In addition, the linear variation is just an approximation and different behaviors are also reported in literatures [22]. The carrier concentration of absorber can be tuned in a range of six orders of magnitude [23], ranging from 10^{13} cm^{-3} to 10^{19} cm^{-3}, and we choose 10^{16} cm^{-3} in our simulation. Since it is not benefit for the light absorption when absorber thickness is too low. However, too thick absorber layer can induce longer transfer route of the photo-generated carriers, leading to higher recombination. Therefore, in our simulation the perovskite thickness is set to be a reasonable value of 500 nm. In each layer, the defect energy level is at the center of the band gap and is set to be in the neutral Gaussian distribution with 0.1 eV characteristic energy. The work function of back and front contact are 5 eV (Carbon) and 4.4 eV (FTO) [14], respectively. Thermal velocities of the hole and electron are set as 10^7 cm/s. In this study, the absorption coefficient, α (cm^{-1}), is calculated according to

$$\alpha = A_\alpha(hv - E_g)^{1/2} \quad (4)$$

where, A_α is absorption constant and is set as 5×10^4 cm^{-1} $eV^{-1/2}$ for the simulation to simplify the simulation model. The SCAPS simulation program uses a dedicated interpolation algorithm [24] to determine the grading of the optical absorption. To simplify the simulation, the impacts of defect states at the interface are not considered. Characterization of the devices is performed under AM1.5 solar spectrum.

Table 1
Material parameters set in the simulation.

Parameters	FTO	ZnO	Perovskite
Thickness(nm)	500	55	500
N_A (cm^{-3})	–	–	10^{16}
N_D (cm^{-3})	2×10^{19} [14]	10^{18} [15]	–
ε_r	9.0	9.0 [15]	10 [17]
χ (eV)	4.0	4.0 [16]	variable
E_g (eV)	3.5	3.3 [16]	variable
μ_n (cm^2/V/s)	20	100	10 [18]
μ_p (cm^2/V/s)	10	25	10 [18]
N_t (cm^{-3})	10^{15} [9]	10^{15}	2.5×10^{13} [14]
N_C (cm^{-3})	2.2×10^{18} [14]	3.7×10^{18} [15]	2.5×10^{20} [14]
N_V (cm^{-3})	1.8×10^{19} [14]	1.8×10^{19} [16]	2.5×10^{20} [14]

3. Results and discussion

3.1. Uniform band gap $CH_3NH_3Pb(I_{1-x}Br_x)_3$ absorber

Device performances of the simulated HTM-free PSCs as a function of band-gap of $CH_3NH_3Pb(I_{1-x}Br_x)_3$ absorber layer are shown in Figs. 2 and 3. The E_g is varied from 1.5 to 2.3 eV, corresponding to Br/(I + Br) (x) ratios range from 0 to 1. It can be observed that the open-circuit voltage (V_{OC}) improves with the increasing of the band gap, while the fill factor (*FF*) and short-circuit current (J_{SC}) drops due to the decrease

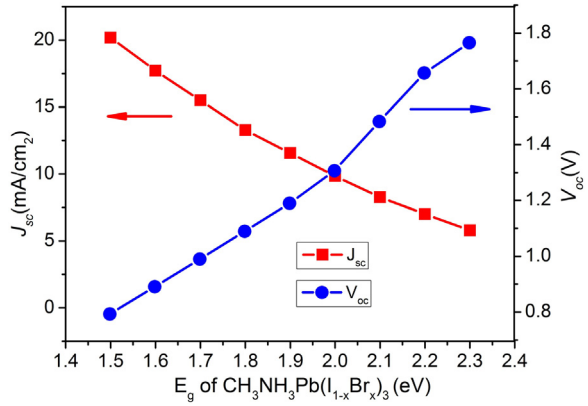

Fig. 2. Variation of V_{OC} and J_{SC} for different $CH_3NH_3Pb(I_{1-x}Br_x)_3$ absorber band gap.

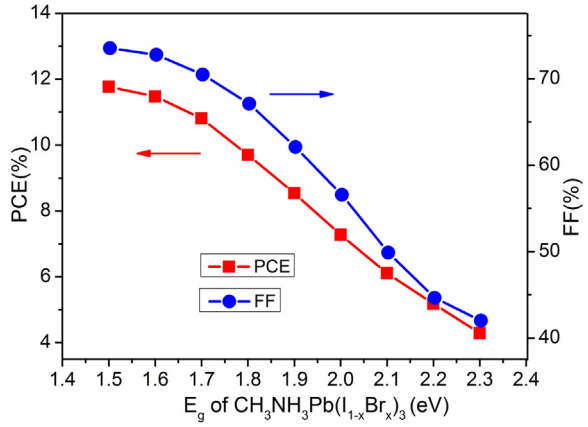

Fig. 3. Variation of *FF* and *PCE* for different $CH_3NH_3Pb(I_{1-x}Br_x)_3$ absorber band gap.

of the light absorption of photons with lower energy than the band gap energy. Only photons with an energy higher than the absorber band gap will give a contribution to the photocurrent.

With the increase of absorber band gap, since only E_c is assumed to shift, therefore, the conduction band offset at absorber/ZnO interface becomes larger, larger gap difference can lead to the larger interface contact resistance [25], which will decrease the fill factor [26]. The power conversion efficiency (*PCE*) exhibit the same variation trend as *FF* and decrease with the band gap. The increase of E_g indicates a worsening of the light harvesting property as the layer composition changing from $CH_3NH_3PbI_3$ to $CH_3NH_3PbBr_3$, therefore a reduced performance of PSCs. Fig. 4 exhibits the trend of quantum efficiency (*QE*) as a function of the E_g. We can find that the *QE* gradually decreases with the increasing of E_g. The reduction of *QE* with increasing E_g is directly related to the blue-shift of absorption onset. In addition, the low *QE* in short wavelength region (< 350 nm) is attributed to the absorption by FTO. Therefore, a uniform band gap $CH_3NH_3Pb(I_{1-x}Br_x)_3$ absorber is non-ideal configuration for PSC. $CH_3NH_3Pb(I_{1-x}Br_x)_3$ is only used as the grading surface layer while keeping the band gap of the main body of the $CH_3NH_3PbI_3$ absorber at the optimum value as 1.5 eV in the following discussion.

3.2. Graded band gap $CH_3NH_3Pb(I_{1-x}Br_x)_3$ absorber

3.2.1. Back grading

Back grading is defined as the band gap increasing toward the back of the absorber layer. The bandgap profile of back grading is shown in Fig. 5(a), where E_{gb} is the band gap at the back surface of absorber and

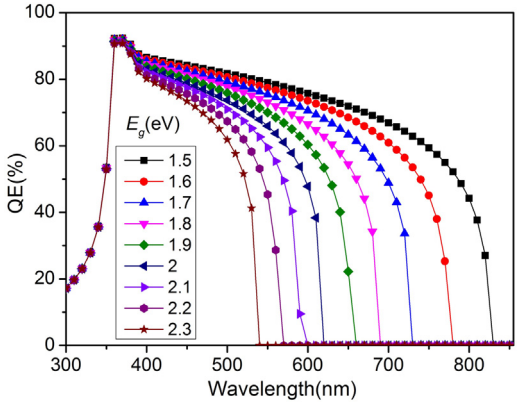

Fig. 4. QE as a function of $CH_3NH_3Pb(I_{1-x}Br_x)_3$ absorber band gap.

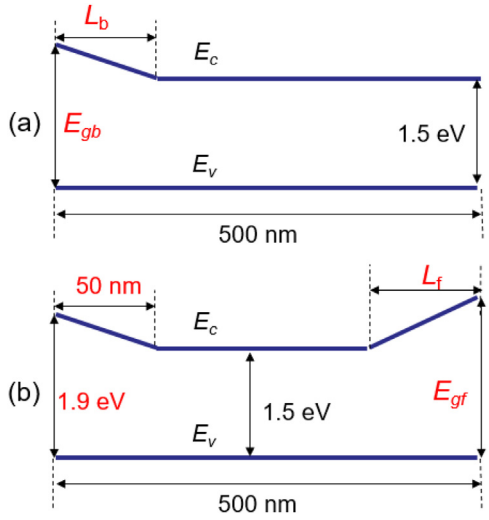

Fig. 5. Schematic of band gap profile used in the simulation (a) back grading; (b) double grading.

L_b is the thickness engineered at the back of $CH_3NH_3Pb(I_{1-x}Br_x)_3$ absorber. The locally enhanced band gap influences the photo-generated minority carriers in two ways: Firstly, in the regions with increasing band gap the probability of recombination will be reduced because the probability is inversely proportional to the E_g [27]. Moreover, an additional quasi-electric field (due to the gradient of electron affinity), *E*, obtained and can be described as following [28],

$$E = \frac{d\Delta E_g}{dL} \tag{5}$$

where ΔE_g is the variation in band gap over the distances L_1 due to Br-grading. For a fixed band gap of 1.5 eV at the front surface of the absorber, in order to optimize the bandgap profile, the back surface band gap E_{gb} is varied from 1.5–2.3 eV, with an interval of 0.2 eV, and combined with a L_b from 50 to 500 nm. The variations of photovoltaic parameters and J-V curves of the HTM-free perovskite solar cells with different L_b as a function of E_{gb} are exhibited in Figs. 6 and 7. The simulation results illustrate that the V_{OC} improves continuously with the increasing E_{gb} from 1.5 to 1.9 eV at all different L_b, however, it becomes an approximate constant after E_{gb} is beyond 1.9 eV. In addition, the J_{SC} first exhibits an improvement with increasing E_{gb} and then decreases slightly when E_{gb} excess 1.9 eV with L_b from 50 to 350 nm. Moreover, the *FF* first shows an enhancement with the increase of E_{gb} at all different L_b and then becomes an approximate constant when E_{gb} beyond 1.9 eV. This phenomenon can be explained as following: The additional electric field introduced by back grading can keep minority

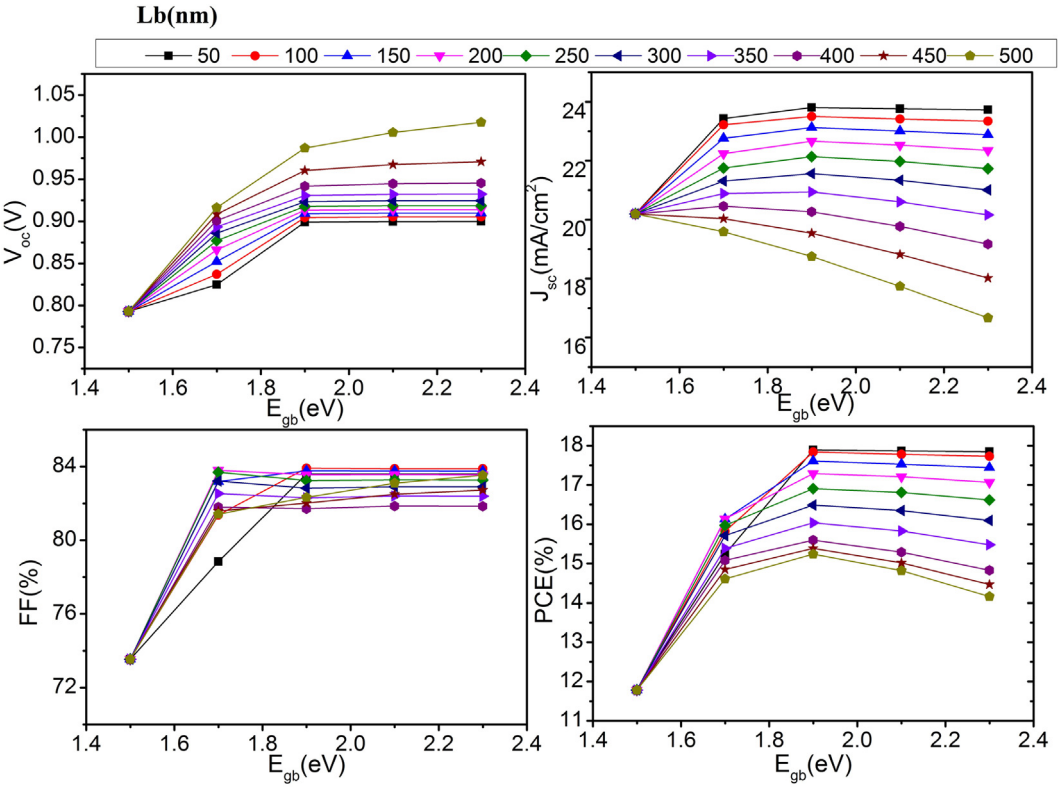

Fig. 6. Variations of photovoltaic parameters of the HTM-free PSCs with different L_b as a function of E_{gb}.

carriers away from the back contact and further prompt the separation of the photon-generated carriers, reduce the recombination rate, which leads to an increase *FF*. The energy band diagrams with different E_{gb} and the transportation process of photo-generated carriers are illustrated in Fig. 8. It can be observed from Fig. 8(a) that when E_{gb} = 1.5 eV the electron will flow from the absorber to back contact since the absorber is a flat conduction band. However, when grading towards the back contact, as shown in Fig. 8(b), the conduction band of higher energy can act as a barrier so that the photo-generated electrons will be returned back to the ZnO, therefore, enhancing the collection of minority carriers in PSCs, both the V_{oc} and the J_{sc} experience fast enhancement. However, V_{OC} exhibits a reduced increase when E_{gb} above 1.9 eV because photons of low energy are absorbed deeply into the absorber near the back contact and not all of the photo-generated minority carriers can reach space charge region even with the additional electric field. Moreover, when L_b is above 400 nm, the J_{SC} decreases continuously with increasing E_{gb} because higher band gap E_{gb} with thicker L_b will lead to lower light absorption. In back grading profile, the optimum efficiency of 17.89% (J_{SC} = 23.8 mA/cm^2, *FF* = 0.84, V_{OC} = 0.9 V) is achieved when E_{gb} = 1.9 eV with L_b = 50 nm.

3.2.2. *Double grading*

In order to further increase the PCE, a double grading configuration is also examined in this work. Double grading is increasing the band gap both towards the front and back contact. The band gap profile of double grading is shown in Fig. 5(b), where E_{gf} is the graded bandgap at the absorber front surface and L_f is the thickness. Based on the above-mentioned simulation results, the optimal performance of the back

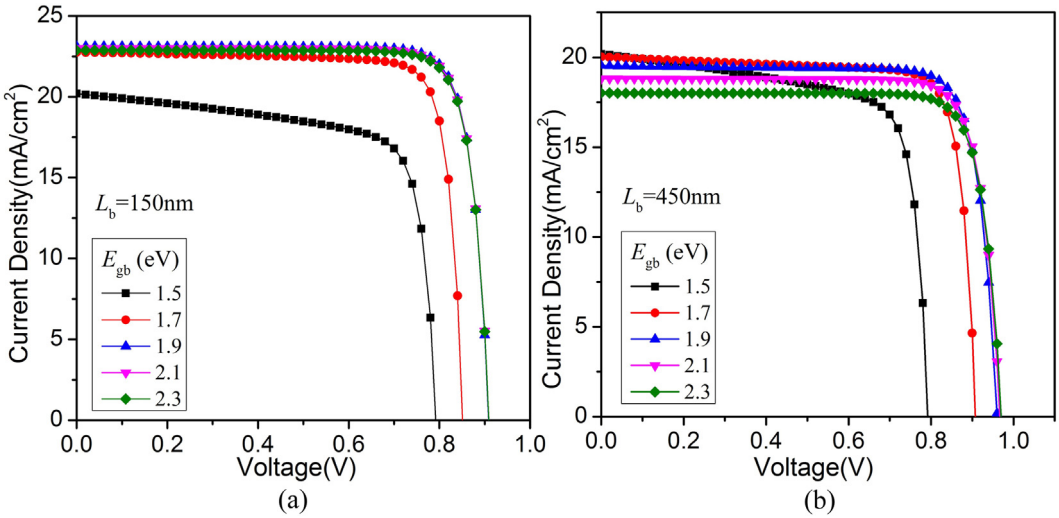

Fig. 7. I-V curves of different E_{gb} with (a) L_b = 150 nm and (b) L_b = 450 nm in HTM-free PSCs.

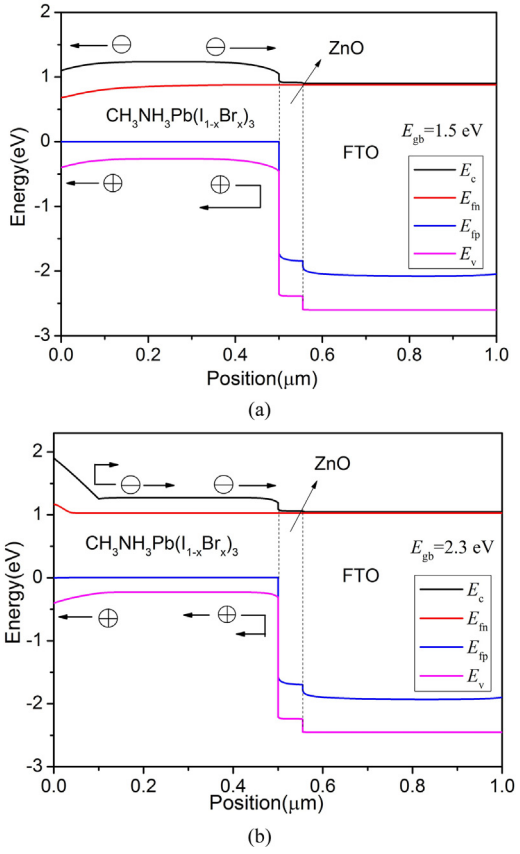

Fig. 8. Energy band diagram of varied E_{gb} (a) E_{gb} = 1.5 eV, and (b) E_{gb} = 2.3 eV with L_b = 100 nm.

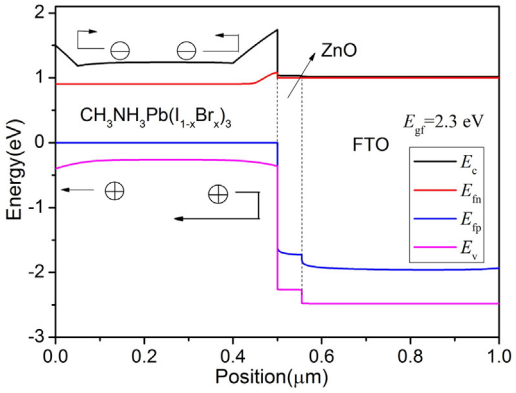

Fig. 10. Energy band diagram of double grading with E_{gf} = 2.3 eV and L_f = 100 nm.

grading is set with L_b and E_{gb} to be 50 nm and 1.9 eV, respectively. Therefore, in this case, the graded thickness L_f is changed from 50 nm to 300 nm and E_{gf} is varied from 1.5 to 2.2 eV, with an interval of 0.1 eV. The variations of device performance of the HTM-free perovskite solar cells with various L_f as a function of E_{gf} are exhibited in Fig. 9. V_{OC} exhibits an enhancement with an increase of E_{gf} from 1.5 to 2.2 eV at different L_f because the increasing E_{gf} enables the built-in potential to increase. However, the increase of E_{gf} leads to a reduction of J_{SC} because the high barrier formed by reverse grading prevents the collection of minority carrier and its height increases with increasing E_{gf}, as can be observed from energy band diagram of double grading illustrated in Fig. 10. The *PCE* and *FF* exhibit the same variation trend. The *PCE* stays high as 17.89% with E_{gf} ranging from 1.5 eV to 1.8 eV when L_f less than 100 nm. However, with further increases in E_{g2}, the *PCE* drops considerably mainly due to the degradation of *FF* when E_{gf} is above 1.8 eV. In addition, with the increase of L_f, the conversion efficiency decreases

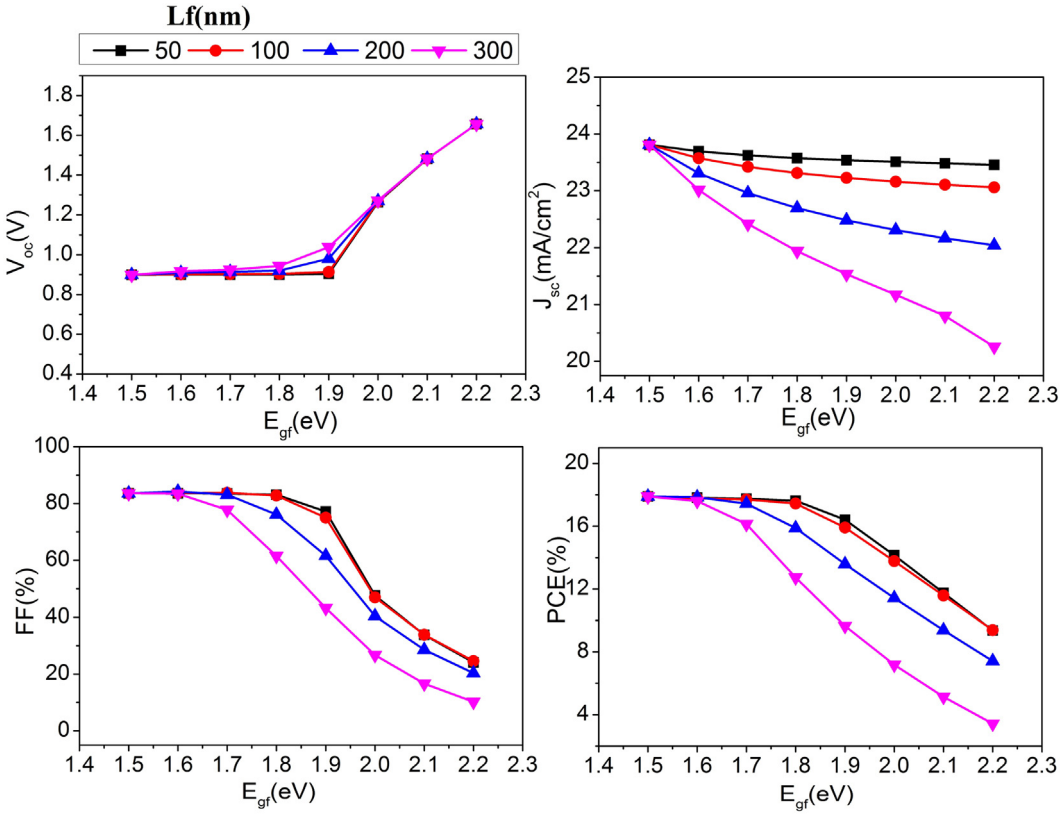

Fig. 9. Variations of photovoltaic parameters of the HTM-free PSCs with different L_f as a function of E_{gf}.

considerably because less carriers can be collected due to thicker front barrier. Therefore, the double grading structure is not beneficial for *PCE* and cannot outperform the back grading structure.

4. Conclusion

In summary, a numerical analysis is performed on the absorber band gap of HTM-free PSCs with carbon electrode using SCAPS-1D. Firstly, we study the influence of varied uniform band gap of $CH_3NH_3Pb(I_{1-x}Br_x)_3$ absorber on device performance. Our simulation results illustrate that device performance drops with the increasing of absorber band gap. Then we analyze the effect of different band gap profile, including double grading and back grading. The results indicate that grading towards the back contact remarkably enhances the device performance and the maximum efficiency is about 17.89% corresponding to a graded layer thickness of 50 nm and with 1.9 eV band gap at back surface. This enhancement is mainly due to the additional electric field introduced by the back grading that impede photo-generated minority carriers transport from the absorber to the back contact. Hence, reducing the recombination at the back contact and enhancing the carrier collection. In addition, the double grading is executed on the basis of the optimum back grading, which modifies the front surface band gap together with the graded thickness. In double grading profile, device performance drops with the increasing band gap of front surface because a high barrier is formed to impede the transportation of electron and improve the recombination rate. This simulation results in this study can indicate the direction for further efficiency enhancement of the low cost perovskite solar cells.

Acknowledgements

We acknowledge the Professor Burgelman's group of the University of Gent, Belgium for providing the SCAPS program and allowing its use. This work is supported by Department of Education, Fujian Province of China (Grant no. JAT170622, JAT170630), Fujian Provincial Department of Science and Technology of China (Grant no. 2015H0010), Natural Science Foundation of Fujian Province (Grant no. 2016J01752) and National Natural Science Foundation of China (Grant no. 51402050).

References

[1] G.E. Eperon, V.M. Burlakov, P. Docampo, A. Goriely, H.J. Snaith, Morphological control for high performance, solution-processed planar heterojunction perovskite solar cells, Adv. Funct. Mater. 24 (2014) 151–157.
[2] J.M. Ball, M.M. Lee, A. Hey, H.J. Snaith, Low-temperature processed mesosuperstructured to thin-film perovskite solar cells, Energy Environ. Sci. 6 (2013) 1739–1743.
[3] M. Liu, M.B. Johnston, H.J. Snaith, Efficient planar heterojunction perovskite solar cells by vapour deposition, Nature 501 (2013) 395–398.
[4] J. You, Z. Hong, Y. Yang, Q. Chen, M. Cai, T.B. Song, C.C. Chen, S. Lu, Y. Liu, H. Zhou, Y. Yang, Low-temperature solution-processed perovskite solar cells with high efficiency and flexibility, ACS Nano 8 (2014) 1674–1680.
[5] J.H. Noh, S.H. Im, J.H. Heo, T.N. Mandal, S.I. Seok, Chemical management for colorful, efficient, and stable inorganic-organic hybrid nanostructured solar cells, Nano Lett. 13 (2013) 1764–1769.
[6] H.W. Zhou, Y.T. Shi, K. Wang, Q.S. Dong, X.G. Bai, Y.J. Xing, Y. Du, T.L. Ma, Low-temperature processed and carbon-based $ZnO/CH_3NH_3PbI_3/C$ planar heterojunction perovskite solar cells, J. Phys. Chem. C 119 (2015) 4600–4605.
[7] J. Even, L. Pedesseau, J.M. Jancu, C. Katan, Importance of spin–orbit coupling in hybrid organic/inorganic perovskites for photovoltaic applications, J. Phys. Chem. Lett. 4 (2013) 2999–3005.
[8] M.A. Contreras, J. Tuttle, A. Gabor, A. Tennant, K. Ramanathan, S. Asher, A. Franz, J. Keane, L. Wang, R. Noufi, High efficiency graded bandgap thin-film polycrystalline $Cu(In,Ga)Se_2$-based solar cells, Sol. Energy Mater. Sol. Cells 41/42 (1996) 231.
[9] T. Dullweber, G. Hanna, U. Rau, H.W. Schock, A new approach to high-efficiency solar cells by band gap grading in $Cu(In,Ga)Se_2$ chalcopyrite semiconductors, Sol. Energy Mater. Sol. Cells 67 (2001) 145.
[10] M. Burgelman, P. Nollet, S. Degrave, Modeling polycrystalline semiconductor solar cells, Thin Solid Films 361 (2000) 527–532.
[11] A. Nicolaev, T.L. Mitran, S. Iftimie, G.A. Nemnes, Optimization of halide perovskite solar cells based on nanocolumnar ZnO, Sol. Energy Mater. Sol. Cells 158 (2016) 202–208.
[12] Q.Z. An, P. Fassl, Y.J. Hofstetter, D. Becker-Koch, A. Bausch, Paul E. Hopkinson, Y. Vaynzof, High performance planar perovskite solar cells by ZnO electron transport layer engineering, Nano Energy 39 (2017) 400–408.
[13] J. Luo, Y.X. Wang, Q.F. Zhang, Progress in perovskite solar cells based on ZnO nanostructures, Sol. Energy 163 (2018) 289–306.
[14] L. Huang, X.X. Sun, C. Li, R. Xu, J. Xu, Y.Y. Du, Y.X. Wu, J. Ni, H.K. Cai, J. Li, Z.Y. Hu, J.J. Zhang, Electron transport layer-free planar perovskite solar cells: further performance enhancement perspective from device simulation, Sol. Energy Mater. Sol. Cells 157 (2016) 1038–1047.
[15] X. Shang, Z. Wang, M. Li, L. Zhang, J. Fang, J. Tai, Y. He, A numerical simulation study of $CuInS_2$ solar cells, Thin Solid Films 550 (2014) 649–653.
[16] M. Nawaz, E.S. Marstein, A. Holt, Design analysis ZnO/cSi heterojunction solar cell, in: Proceedings of the IEEE Photovoltaic Specialist Conference (PVSC) Honolulu, 20–25 June, 2010, pp. 2213–2218.
[17] C.C. Homes, Optical response of high-dielectric-constant perovskite-related oxide, Science 293 (2001) 673–676.
[18] C. Wehrenfennig, G.E. Eperon, M.B. Johnston, H.J. Snaith, L.M. Herz, High charge carrier mobilities and lifetimes in organolead trihalide perovskites, Adv. Mater. 26 (2014) 1584–1589.
[19] A. Kojima, K. Teshima, Y. Shirai, T. Miyasaka, Organometal halide perovskites as visible-light sensitizers for photovoltaic cells, J. Am. Chem. Soc. 131 (2009) 6050–6051.
[20] H.S. Kim, C.R. Lee, J.H. Im, K.B. Lee, T. Moehl, A. Marchioro, S.J. Moon, R. Humphry-Baker, J.H. Yum, J.E. Moser, et al., Lead iodide perovskite sensitized all-solid-state submicron thin film mesoscopic solar cell with efficiency exceeding 9%, Sci. Rep. 2 (2012) 591.
[21] Y.T. Liu, T.H. Chen, C.C. Lin, C.M. Fan, J.C. Liu, Y.L. Tung, S.Y. Tsai, Modeling and simulation of band-gap profling with planar heterojunction of hole-transporting layer-free perovskite solar cells, Mater. Res. Express 4 (2017) 075505.
[22] U.G. Jong, C.J. Yu, J.S. Ri, N.H. Kim, G.C. Ri, Influence of halide composition on the structural, electronic, and optical properties of mixed $CH_3NH_3Pb(I_{1-x}Br_x)_3$ perovskites calculated using the virtual crystal approximation method, Phys. Rev. B 94 (2016) 125139.
[23] Q. Wang, Y. Shao, H. Xie, L. Lyu, X. Liu, Y. Gao, J. Huang, Qualifying composition dependent p and n self-doping in $CH_3NH_3PbI_3$, Appl. Phys. Lett. 105 (2014) 163508.
[24] M. Burgelman, J. Marlein, Analysis of graded band gap solar cells with SCAPS, in: Proceedings of the 23rd European Photovoltaic Solar Energy Conference, Valencia, 2008, pp. 2151–2155.
[25] H.J. Du, W.C. Wang, Y.F. Gu, Simulation design of P–I–N-type all-perovskite solar cells with high efficiency, Chin. Phys. B 26 (2) (2017) 028803.
[26] B.Y. Qi, J.Z. Wang, Fill factor in organic solar cells, Phys. Chem. Chem. Phys. 15 (2013) 8972.
[27] M.A. Green, Solar Cells: Operating Principles, Technology and System Applications, The University of New South Wales, Kensington, 1992, p. 50 (142).
[28] O. Lundberg, Ph.D. thesis, Uppsala University, 2003, ISBN 91-544-5790-8. ⟨http://publications.uu.se/thesis/abstract.xsql?Dbid = 3757⟩.